RESEARCH ACTIVITIES VI
Department of Vacuum UV Photoscience

VI-A Electronic Structure and Decay Mechanism of Inner-Shell Excited Molecules

In this project, we have two major subjects: (a) resonant photoelectron spectroscopy and (b) resonant inelastic soft X-ray emission spectroscopy following inner-shell excitations of simple molecules. We have already found some spin-forbidden ionized and excited states in (a) and (b) in collaboration with Uppsala University and Advanced Light Source. In the spectral assignments, angle(symmetry)-resolved photoion yield techniques and theoretical calculations are essential. We are now developing an original soft X-ray emission spectrometer for the recently upgraded UVSOR facility.

VI-A-1 Design and Development of a Novel Transmission Grating Spectrometer for Soft X-Ray Emission Studies

HATSUI, Takaki; SETOYAMA, Hiroyuki; SHIGEMASA, Eiji; KOSUGI, Nobuhiro

[*AIP Conference Proceedings* in press]

High resolution soft x-ray emission spectroscopy (XES) in combination with synchrotron radiation as an exciting source has been extensively studied. We propose a novel spectrometer design for high resolution soft-x-ray emission studies. Figure 1 shows the schematic layout of a transmission-grating spectrometer (TGS). In order to focus the emitted x-ray both horizontally and vertically, a Wolter type I mirror is introduced as the prefocussing mirror with a magnification of 10. The grazing-incidence angle of 1 degree gives a collection angle of 1.5×10^{-3} sr. A free-standing transmission plane grating with its groove density of 10000 lines/mm is placed at 67 mm downstream of the edge of the Wolter mirror, in the normal incidence geometry. A back-illuminated CCD, whose position is changed along the Rowland torus with scanning the photon energy, is located at 1400 mm downstream from the grating. In order to evaluate the aberrations of TGS, a ray-tracing code TGSGUI is developed by one of the authors (T.H.). Figure 2 shows a spot diagram of the 1st order diffracted rays of 320 eV at the detector with a rectangular source of 1(v.) × 200(h.) μm^2. The plane figure of the grating causes aberrations.[1] The diagram however indicates that the resolving power better than 5000 is possible. The spatial resolution of the detector however should be very high, which is estimated to be about 1 μm, in order to achieve such a high resolution. The novel TGS is very promising because of its large collection angle and high energy resolution. Technical difficulties in realization of transmission gratings and high spatial resolution CCD still remain to be solved. The optical elements are now under development.

References

1) K.P. Beuermann, *et al., Appl. Opt.* **17**, 2304 (1978).

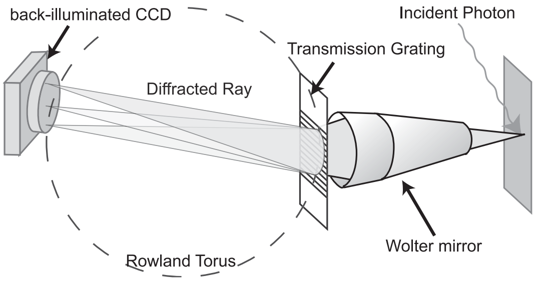

Figure 1. Schematic layout of the transmission-grating spectrometer (TGS).

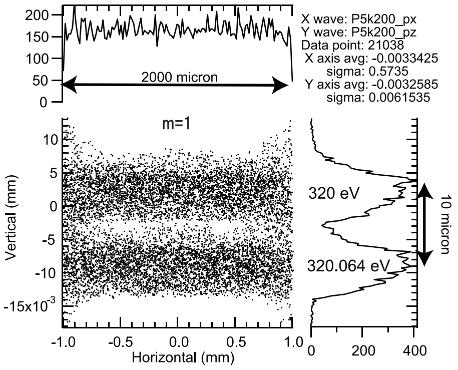

Figure 2. Spot diagram of the 1st order diffracted rays of 320 eV at the detector with a rectangular source of 1(v.) × 200(h.) μm^2.

VI-A-2 Symmetry-Resolved Photoion Yield Spectra of N_2 and C_2H_2

MASUDA, Suomi[1]; GEJO, Tatsuo[2]; KOSUGI, Nobuhiro
([1]*GUAS;* [2]*Himeji Inst. Tech.)*

In homonuclear systems, core excited states have a gerade-ungerade splitting. It has been discussed in term of delocalization of the core hole through the core-valence interaction between adjacent atoms.[1] Relatively large g-u splitting is reported for N_2 and C_2H_2.[2] In this work, we applied angle-resolved photoion yield spectroscopy (ARPIS) to core to Rydberg excitation of N_2 and C_2H_2 to study core excitation below the ionization thresholds. Because photo-excitation has the g-u selectivity, ARPIS can provide information on the symmetry of the excited states. ARPIS of N_2 and C_2H_2 near the N and C *K*-edge region are shown in Figure 1 and 2, respectively. In both the spectra, the parallel and perpendicular transitions are clearly resolved. Two ionization thresholds $^2\Sigma_g^+$ and $^2\Sigma_u^+$ are determined to have $\Delta_{gu} = 109 \pm 8$ meV and $\Delta_{gu} = 119 \pm 15$ meV for N_2 and C_2H_2 by extrapolating each Rydberg series by using Rydberg formula for a hydrogen-like system combined with constant quantum defects. In Figure 2, distinct difference is observed between vibrational progressions of $3p\sigma_u$ and those of $3p\pi_u$. In the $3p\sigma_u$ Rydberg excited state, the C–H symmetric stretching mode ν_1 is excited in addition to the C–C symmetric stretching mode ν_2. It can be attributed to perturbation in the $3p\sigma_u$ Rydberg excited state from the $3\sigma^*_u$ valence excited state, which has the C–H antibonding character.

References

1) N. Kosugi, *Chem. Phys.* **289**, 117 (2003).
2) B. Kempgens, *et al., Phys. Rev. Lett.* **79**, 19 (1997).

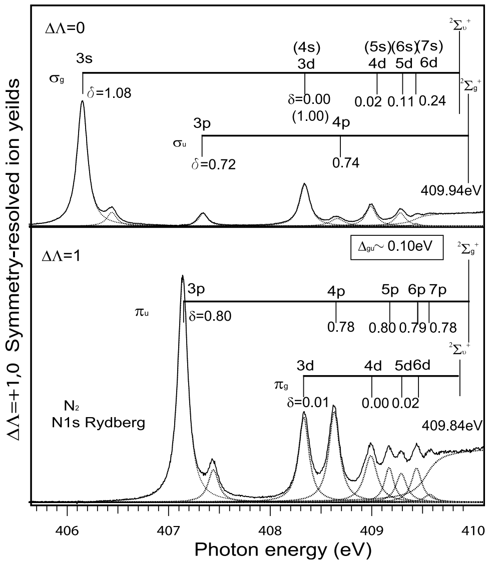

Figure 1. ARPIS of N_2 measured at near N *K*-edge region.

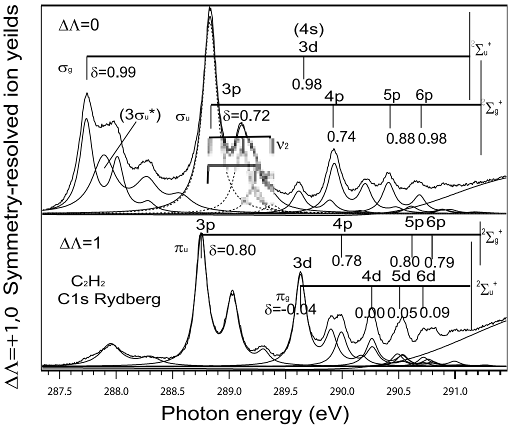

Figure 2. ARPIS of C_2H_2 measured at near C *K*-edge region.

VI-A-3 Ab Initio R-Matrix/MQDT Method for Near-Edge X-Ray Absorption Fine Structure

HIYAMA, Miyabi[1]; KOSUGI, Nobuhiro
(*[1]Univ. Tokyo)*

[*Phys. Scr.* in press]

We have investigated feasibility of an ab initio polyatomic R-matrix/MQDT (multichannel quantum defect theory) method1) using Gaussian type basis functions for the bound and continuum states to analyze the near edge feature of molecules. Test molecules here are N_2, C_2H_2, and NO. The R-matrix/MQDT method is revealed to be indispensable for the Rydberg states with the higher quantum number and the continuum states, both of which cannot be described by using Gaussian type functions in the outer region from an appropriate boundary. The close-coupling calculation augmented with the correlation term, which is carried out for the inner region, is powerful to describe the valence states and the interchannel coupling in several core-ionized states.

Reference

1) M. Hiyama and M. S. Child, *J. Phys. B* **35**, 1337 (2002).

VI-B Soft X-Ray Photoelectron-Photoabsorption Spectroscopy and Electronic Structure of Molecular Solids and Clusters

This project has been carried out in collaboration with Wuerzburg University. We have two subprojects: (a) molecules and radicals in condensed phase and in rare gas matrix, and (b) ionic fragmentations of molecular clusters following the inner-shell resonance excitation. In (a), we have measured Ar 2*p* excitation spectra in some matrix phases at the bending-magnet beamline BL4B of the UVSOR facility. In (b), we are developing a new cluster source for photoelectron measurements on a newly constructed undulator beamline BL3U.

VI-B-1 Ar 2*p* Excited States of Argon in Non-Polar Media

HATSUI, Takaki; NAGASONO, Mitsuru[1]; KOSUGI, Nobuhiro
(*[1]Kyoto Univ.)*

[*J. Electron Spectrosc. Relat. Phenom.* in press]

Rydberg states in condensed phase are sensitive to external perturbation due to their large orbital radii. In the present study, Ar 2*p* excitations of solid Ar, and Ar:Kr, Ar:Xe and Ar:N_2 mixtures are investigated with high energy resolution in order to clarify the nature of Rydberg excited states in non-polar media. Figure 1 shows Ar 2*p* photoabsorption spectra of Ar gas, solid Ar, and Ar:Kr(1:4) and Ar:Xe(1:4) mixtures. The solid Ar spectrum shows Rydberg excitations blue-shifted compared with the Ar gas, as reported in the earlier work.1) The lowest Ar $2p_{3/2}$-4*s* band has a shoulder structure on the lower energy side. In order to discriminate surface contribution from bulk, fluorescence yield was measured for solid Ar (dotted line). The spectral features are very similar except for the shoulder and a weak band observed around 246.14 eV, which are clearly suppressed in the fluorescence yield spectra. They are hence assigned to the excitations arising from surface Ar atoms. The shoulder at ~ 244.6 eV can be assigned to the surface Ar $2p_{3/2}$-4*s* excitation. On the other hand, the weak band at ~ 246.14 eV can be assigned to the surface Ar $2p_{3/2}$-4*p* excitation, which becomes dipole allowed because of the lower local symmetry of surface Ar atoms. The bulk Ar $2p_{3/2}$-4*p* is not observable. The feature at 247–248.5 eV is broadened mainly because of the overlap of *nd* excitations. The bulk Ar $2p_{3/2}$-4*s* band in the Ar:Kr (1:9) spectrum locates at 244.82 eV with a red shift of 0.24 eV in comparison with the bulk Ar $2p_{3/2}$-4*s* band in the Ar solid. The red shift in the Ar:Kr mixture compared to the Ar solid can be explained as a combination of two effects, namely, decrease of ionization threshold and increase of term value. The ionization threshold is lowered in condensed phase by polarization stabilization. Based on a continuum model that treats all surrounding atoms as dielectric continuum, the ionization threshold for Ar:Kr mixture is predicted to be lower than that for Ar solid. On the other hand, the exchange repulsion of the excited Rydberg electron by the valence electrons of the neighboring atoms is predominantly determined by the distance between the core-excited atom and the neighboring atoms. Longer interatomic distance of Ar–Kr than Ar–Ar, results in smaller exchange repulsion. The excited states in Ar:Kr mixture hence have larger term values (lower excitation energies) than the Ar solid. Both the larger polarization stabilization and the smaller exchange repulsion make the excitation energies for Ar:Kr mixtures lower than those for Ar solid. Similar arguments are possible for Ar:Xe mixtures. Both the larger polarization stabilization and the smaller exchange repulsion contribute to larger red shift in Ar:Xe than in Ar:Kr. In the case of Ar:N_2 mixtures, Ar $2p_{3/2}$-4*s* band shows small red shift to the Ar solid, which is explained as a balance between the red shift by the polarization stabilization and the blue shift arising from the exchange repulsion. On the contrary, the Ar $2p_{3/2}$-*nd* band in Ar:N_2 mixtures shows a large blue shift to the Ar solid, which is explained by the strong exchange repulsion of spatially extended *nd* electrons by N_2 with short Ar–N distances.

Reference

1) R. Haensel, *et al.*, *Phys. Rev. B* **7**, 1577 (1973).

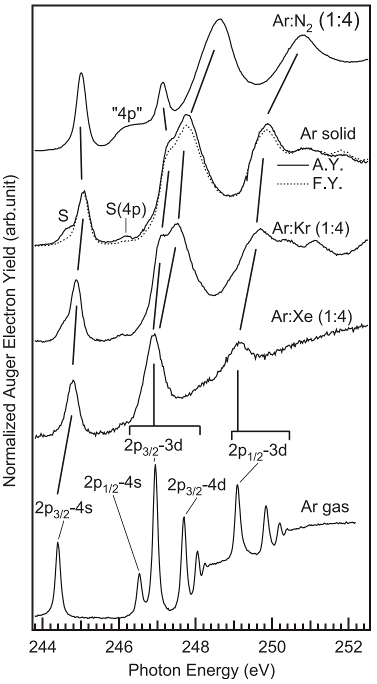

Figure 1. Ar 2*p* excitation spectra measured by using Auger electron yield method for Ar gas, Ar solid, and Ar:Kr(1:4), Ar:Xe(1:4) and Ar:N_2(1:4) mixtures. Fluorescence yield spectrum for Ar solid is shown as dotted line.

VI-B-2 Development and Construction of a Novel Undulator Beamline BL3U for Soft X-Ray Emission Studies

HATSUI, Takaki; SETOYAMA, Hiroyuki; MASUDA, Suomi; SHIGEMASA, Eiji; KOSUGI, Nobuhiro

[*AIP Conference Proceedings* in press]

A soft x-ray emission spectrometer (XES) generally requires small beam size at the sample position, because a smaller opening of the spectrometer entrance slit is needed to achieve higher energy resolution. Such a beam is usually produced by refocusing optics downstream of the exit slit. In our case, the adoption of such refocusing optics is impossible, due to a very limited space. On the other hand, a monochromator with short arm lengths is utilized with a small exit-slit opening for obtaining practical resolution. It is feasible to carry out XES studies at the exit slit position, if the monochromator has a constant exit-arm length. We have designed a varied-line-spacing plane (VLSP) grating monochromator in order to satisfy high energy resolution of $\lambda/\Delta\lambda = 10^4$ and small width of the exit slit opening. Figure 1 represents the layout of the beamline BL3U at the UVSOR facility. The cylindrical mirror M0 vertically focuses the beam on the entrance slit S0 with the demagnification of 1/7.57. Because of the short arm length, the entrance-slit opening corresponding to the resolving power of $\lambda/\Delta\lambda = 10^4$ becomes smaller than the beam size. This mismatch causes the beam loss of

12–63%. Varied-line-spacing parameters are calculated by minimizing the aberrations in the energy range of interest. The analytical solution of the aberrations for an S0-M1-VLSP-S1 optical system derived by Amemiya *et al.*1) is used. The obtained parameters give resolving power higher than $\lambda/\Delta\lambda = 10^4$ in the photon energy range of 50–800 eV by using three interchangeable gratings with the center groove densities of 1200, 600, and 240 l/mm. In XES setup, the beam is horizontally focused on the exit slit by a plane-elliptical mirror M3, which is located downstream of the VLSP gratings. A sample is placed at 5–10 mm downstream of the exit slit S2. In the case of the multi-purpose setup, the beam is focused on the exit slit S1 only vertically and then refocused in the both directions on the sample by a toroidal mirror M2. The M3 mirror and the exit slit S2 are designed to be interchangeable with the exit slit S1. The calculated photon flux at the sample position in the multi-purpose setup is shown in Figure 2. The XES setup is also calculated to have very similar flux. The beam on the sample in the XES setup has a gaussian distribution with FWHM of 60 μm horizontally. The vertical beam size is close to the opening of the exit slit S2. Due to the diffraction by the exit slit S2, the vertical size of the beam cannot become smaller than ~ 10 μm. The beamline is now under commissioning and will be operated from March 2004.

Reference

1) K. Amemiya, *et al.*, *J. Synchrotron Radiat.* **3**, 282 (1996).

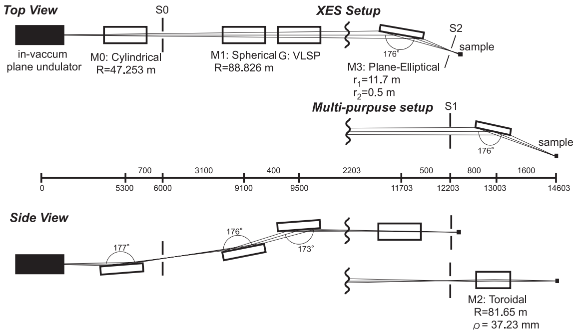

Figure 1. Schematic layout of the BL3U at UVSOR-II. The distances along the beam from the center of the in-vacuum plane undulator are shown in mm. S1X and M2X can be replaced with the other exit slit S1 so that experiments can be carried out at either the XES or multi-purpose endstation. In XES setup, the sample is placed at 5–10 mm downstream of S1X.

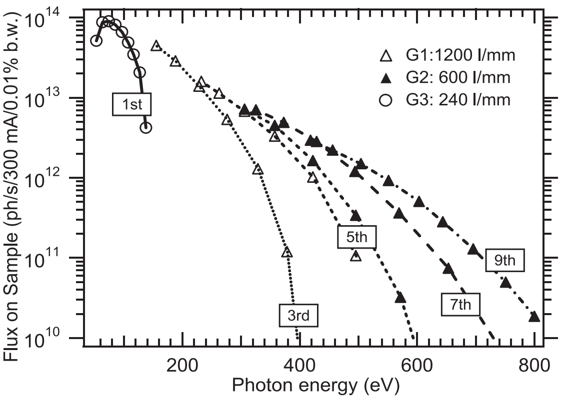

Figure 2. Calculated photon flux at the sample position in multi-purpose setup with the resolving power of $\lambda/\Delta\lambda = 10^4$.

VI-C Synchrotron Radiation Stimulated Surface Reaction and Nanoscience

Synchrotron radiation (SR) stimulated process (etching, CVD) has excellent characteristics of unique material selectivity, low damage, low contamination, high spatial resolution, and high precision *etc*. In this project, nano-level controlled structures are created by using synchrotron radiation stimulated process, and the reaction mechanisms are investigated by using STM and AFM. Concerning the SR etching, we are considering to apply this technique to the microfabrication of integrated protein transistor circuits.

VI-C-1 Design and Performance of Undulator Beamline (BL7U) for In-Situ Observation of Synchrotron Radiation Stimulated Etching by STM

NONOGAKI, Youichi; KATOH, Masahiro; SHIGEMASA, Eiji; MATSUSHITA, Kouji; SUZUI, Mitsukazu; URISU, Tsuneo

[*AIP Conference Proceedings* in press]

An undulator beamline of BL7U equipped with an ultra-high vacuum STM system is constructed at the UVSOR facility to investigate excitation energy dependence in synchrotron radiation stimulated etching. A schematic drawing of BL7U is shown in Figure 1. The SR beam is focused using two cylindrical mirrors on a sample surface just under the STM tip. The photon flux density is calculated to be 10^{19} photons (cm^2 sec 100mA)$^{-1}$ within the spot of 0.67 mm (H) × 0.17 mm (V) on the sample surface at the first harmonic tuned to 100 eV. The hydrogen adsorbed Si(111) surfaces were investigated using the STM apparatus before the undulator irradiation experiments were performed. We successfully observed the etching reaction from rest-atom monohydride surface by hydrogen exposure at room temperature.

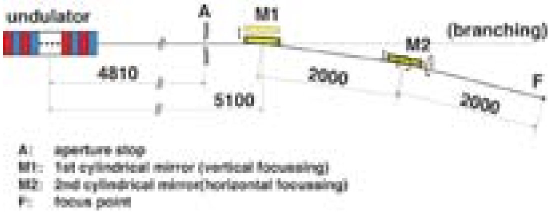

Figure 1. Schematic drawing of BL7U.

VI-C-2 Three-Dimensional Fine Structure on SOG/Si Surface Fabricated by Focused Ion Beam Mask Patterning and Synchrotron Radiation Etching

TERO, Ryugo; RAHMAN, Md. Mashiur; OKAWARA, Hiroshi[1]; NAGAYAMA, Kuniaki[1]; URISU, Tsuneo
([1]CIBS)

Synchrotron radiation (SR) etching of SiO_2 is a unique device process technique.1) The advantages of SR etching are unique material-selectivity, anisotropicity (vertical side wall) and low contaminations.1),2) When SiO_2 surfaces are patterned by SR etching using a contact mask,2) spatial resolution is limited by the available size of the photomask. Focused ion beam (FIB) is one of promising techniques which can make nano-scale patterning on metal, insulator and semi-conductor materials.3) Therefore, nano-processing utilizing the advantages of SR etching will become practicable by applying FIB technique to patterning of etching mask. We have tried for the first time a new three dimensional fine process applying FIB and SR etching methods on spin-on glass (SOG), which is a widely used material in semiconductor processes because planar film with low dielectric constant is easily obtained.

SOG films with thickness of 450–500 nm were obtained after spin-coating on 14 mm square Si wafers followed by curing under flowing N_2 at 698 K for 30 min. SR etching was performed in UHV chamber in BL4A2, under mixture of 2.66×10^{-3} Pa of O_2 and 6.65×10^{-2} Pa of SF_6. Ion beam milling was carried out using 31 keV Ga FIB with a beam spot size of ~ 0.1 μm.

Experiments were performed as followed. First, the SOG film was covered by a Co layer with thickness of ~ 200 nm. Then, the Co photomask was patterned with FIB and the sample was exposed to SR. At last, the Co layer was removed by 0.01 M HNO_3 *aq*. Figure 1 shows an AFM image of the SOG surface after SR etching (2.0×10^4 mA min) followed by removal of the Co layer. Three-dimensional double-step well was successfully obtained in single irradiation process. The Co mask (~ 200 nm thick) was excavated by FIB before irradiation process in the region A and B; Co mask was penetrated to SOG therefore SOG was directly exposed to SR in A; Co mask in B was dug by only 95 nm, which meant FIB milling was stopped in the middle of the Co layer. The AFM profile in Figure 1 clearly shows that the SOG film has been removed and the Si substrate has appeared in the region A. In the region B, the SOG shrank maybe due to a curing effect by penetrating light through the thin Co layer.

Nanometer scale patterning by this combination method is aimed in the future. Effect of diffusion rate of etching gas and interference of light would also be investigated because these factors possibly become important in nano-scale processing.

References

1) T. Urisu and H. Kyuragi, *J. Vac. Sci. Technol., B* **5**, 1436–1440 (1987).
2) H. Akazawa, J. Takahashi, Y. Utsumi, I. Kawashima and T. Urisu, *J. Vac. Sci. Technol., A* **9**, 2653–2661 (1991).
3) S. Reyntjens and R. Puers, *J. Micromech. Microeng.* **11**,

287–300 (2001).

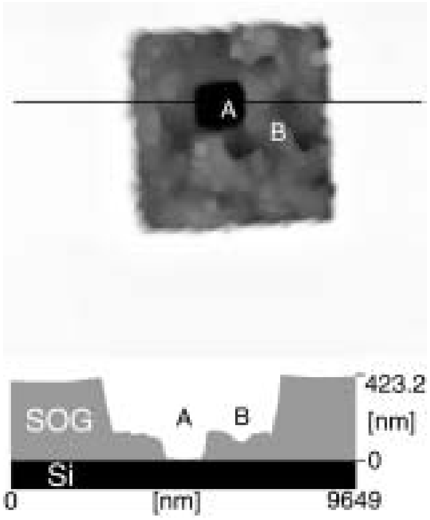

Figure 1. AFM image (10 × 10 μm^2) and a line profile of the SOG/Si surface after SR etching.

VI-C-3 Shrinking of Spin-on-Glass Films Induced by Synchrotron Radiation and Its Application to the 3-D Microfabrications

RAHMAN, Md. Mashiur; TERO, Ryugo; URISU, Tsuneo

[*Jpn. J. Appl. Phys.* to be submitted]

Spin-on-glass (SOG) is an important material in the semiconductor integrated circuit fabrication and widely used for flattening of the inter level dielectrics. Typical thicknesses of SOG films are hundreds of nanometers. It is usually cured with reducing the thickness by heating to high temperatures (for examples at 400 °C–500 °C) in the last stage of the processes. In the present work, we have found that the thickness is also reduced by the irradiation of the synchrotron radiation (SR) beam with covering the surface by Co mask. We are considering that this phenomenon is applied to three-dimensional microfabrications, since the degree of the shrinking depends on the thickness of the mask.

A commercial siloxane type SOG (Honeywell, Accuglass 312B) was used in this study. SOG was spun on 14 mm^2 silicon wafer at a spin speed of 3000 rpm for 10 sec. Immediately after spin coating, the film were subjected to three stages of soft baking on hot plates at 80 °C, 150 °C and 250 °C for 1 min at each temperature. The final curing was performed at 425 °C with a nitrogen gas flow of approximately 1.0 liters/min. After these curing process, thickness of SOG film was approximately 550 nm on Si wafer.

The SR etching of SOG was performed under mixture gas of SF_6 (0.05 Torr) and O_2 (0.002 Torr) at room temperature using a Co mask. The Co contact mask on SOG surface was fabricated by deposition of Co thin film (230 nm) on a resist pattern which was made by the photolithography and lift off technique. The thicker Co mask pattern area was formed by additional deposition of 330 nm Co film. After 20000 mA min dose of SR etching the Co mask was removed by 0.1 N HNO_3 for 3 min. The surface structure was measured by step profilometer (Dektak).

The open region of SOG film was completely etched and the etching was neatly stopped on the Si surface as reported by Urisu and Kyuragi. At the region covered by the thinner Co mask (230 nm), the thickness of SOG film reduced by 152 nm. At the region covered by thicker Co mask, no shrinkage was observed.

The SR etching rate of SOG was investigated. Etched depth of SOG gradually increased with the SR dose. In the present experiment we found that SOG thickness was reduced by the SR etching with thin Co mask and the SR shrinkage of SOG can be controlled with the Co mask thickness. Using this phenomenon we can make three-dimensional structures by one time of SR exposure.

VI-D Noble Semiconductor Surface Vibration Spectroscopy

As a new high sensitive and high resolution surface vibration spectroscopy technique, we are developing an infrared reflection absorption spectroscopy using buried metal layer substrate (BML-IRRAS), which have unique characteristics of high resolution and high sensitivity at finger print regions. Several Si surface chemical reactions are investigated using this BML-IRRAS. As a new fabrication technique of BML substrate, we have almost succeeded in developing the wafer bonding technique. It is considered that BML-IRRAS is also extremely useful in the research of bio-material integration on Si substrates.

VI-D-1 Three Pairs of Doublet Bands Assigned to SiH_2 Scissoring Modes Observed in H_2O-Induced Oxidation of Si(100) Surfaces

WANG, Zhi-Hong; URISU, Tsuneo; NANBU, Shinkoh; MAKI, Jun; GANGAVARAPU, Ranga Rao[1]; AOYAGI, Mutsumi[2]; WATANABE, Hidekazu[3]; OOI, Kenta[3]
([1]IMS and Indian Inst. Tech.; [2]Kyushu Univ.; [3]Natl. Inst. Adv. Ind. Sci. Tech.)

[*Phys. Rev. B* accepted]

Oxidation of Si(100) surfaces by H_2O has been investigated on 2H + H_2O/Si(100)-(2×1), H_2O + Si(100)-(2×1) as well as H_2O + H/Si(100)-(2×1) systems by infrared reflection absorption spectroscopy using $CoSi_2$ buried metal layer substrates (BML-

IRRAS). Three pairs of new doublet bands assigned to the scissoring modes of adjacent and isolated SiH_2 with zero, one and two inserted back bond oxygen atoms, respectively, have been reported for the first time. This is also the first report that has clearly shown the unique high sensitivity of BML-IRRAS for the perpendicular components in the finger print region compared to the multiple internal reflection and the external transmission arrangements. New oxidation mechanisms have been proposed. In the 2H + H_2O/Si(100)-(2×1) system, oxygen insertion into the back bond occurs easily. In the H_2O + H/Si(100) system, however, the tunneling effect is important to reach the oxygen inserted state.

VI-D-2 Assignment of Surface IR Absorption Spectra Measured in the Oxidation Reactions: 2H + H_2O/Si(100) and H_2O + H/Si(100)

WANG, Zhi-Hong; URISU, Tsuneo; GANGAVARAPU, Ranga Rao[1]; NANBU, Shinkoh; MAKI, Jun; AOYAGI, Mutsumi[2]; WATANABE, Hidekazu[3]; OOI, Kenta[3]
([1]IMS and Indian Inst. Tech.; [2]Kyushu Univ.; [3]Natl. Inst. Adv. Ind. Sci. Tech.)

[*Phys. Rev. B* to be submitted]

Infrared reflection absorption spectroscopy using buried metal layer substrates (BML-IRRAS) and density functional cluster calculations have been employed to study the water related oxidation reactions of 2H + H_2O/Si(100)-(2×1), 2D + H_2O/Si(100)-(2×1) and H_2O + H/Si(100)-(2×1). In addition to the oxygen inserted coupled monohydrides reported earlier in the former reaction system, we report several other oxidized Si hydride species in our BML-IRRAS experiments. Three pairs of new vibrational bands are identified between 900 and 1000 cm^{-1} region. These vibrational frequencies have been calculated using Si9 and Si10 cluster models which include all possible structures from zero to five oxygen insertions into the top layer silicon atoms using B3LYP gradient corrected density functional method with polarized 6-31G** basic set to all atoms. The three pairs of vibrational modes are assigned to the scissoring modes of adjacent and isolated SiH_2 with zero, one and two oxygen atoms inserted into the Si back bonds. All the other observed vibrational peaks related to Si oxidation have also been assigned in this study.

VI-D-3 A Comparative Infrared Study of H_2O Reactivity on Si(100)-(2x1), (2x1)-H, (1x1)-H and (3x1)-H Surfaces

GANGAVARAPU, Ranga Rao[1]; WANG, Zhi-Hong; URISU, Tsuneo
([1]IMS and Indian Inst. Tech.)

[*Surf. Sci.* submitted]

Water adsorption on bare and H-terminated Si(100) surfaces has been studied by BML-IRRAS technique. It is found that H-terminated surfaces are much less reactive compared to bare silicon surfaces. The (1×1)-H and (3×1)-H surfaces show similar and less reactivity pattern compared to the (2×1)-H surface. At higher exposures, water reaction with coupled monohydride species provides an effective channel for oxygen insertion into the back bonds of dihydride species.

VI-D-4 Theoretical Analysis of the Oxygen Insertion Process in the Oxidation Reactions of H_2O + H/Si(100) and 2H + H_2O/Si(100); Calculation of an Ab Initio Molecular Orbital Method and an Analysis of the Tunneling Reaction

WATANABE, Hidekazu[1]; NANBU, Shinkoh; WANG, Zhi-Hong; MAKI, Jun; URISU, Tsuneo; AOYAGI, Mutsumi[2]; OOI, Kenta
([1]Natl. Inst. Adv. Ind. Sci. Tech.; [2]Kyushu Univ.)

[*Chem. Phys. Lett.* submitted]

The reaction paths were analyzed, by an ab initio molecular orbital method, for the surface reaction systems, 2H + H_2O/Si(100)-(2×1) and H_2O + H/Si-(100)-(2×1), in which SiH_2 species with one or two oxygen atom-inserted back bonds have been observed as new stable reaction products. It was found that common metastable states exist in both systems, and the initial energy is sufficiently higher than all transition state energies in the former system, while in the latter system, the energy of the highest transition state is much higher than the initial energy, and thus a tunneling effect plays an important role.

VI-D-5 Structure-Optimized $CoSi_2$-Buried-Metal-Layer Substrates for IRRAS Fabricated by Wafer-Bonding

YAMAMURA, Shusaku; YAMAUCHI, Shouichi[1]; WATANABE, Satoru[2]; URISU, Tsuneo
([1]DENSO Res. Lab.; [2]Fujitsu Lab.)

The conventional infrared reflection absorption spectroscopy (IRRAS) is applicable only on the metal substrates. We are developing the IRRAS of semiconductor surfaces using buried metal layer (BML) substrates fabricated by wafer-bonding technique. To obtain high sensitivity in BML-IRRAS, it is essentially important to control the top Si layer thickness less than 200 nm. In this work, we have successfully fabricated BML substrates with 200 nm top Si layer by wafer-bonding technique for the first time using SOI wafers of which Si layer thickness is controlled definitely. Comparing with the ion implantation method, the wafer-bonding method has advantages of (1) atomically flat and (2) low-damaged top Si surfaces without epitaxial growth, which is essentially required in the ion implantation method to remove the ion implantation damage. The preliminary formation of thin (100 nm) SiO_2 layer on the SOI surface was effective to reduce the interface roughness between the top Si and the $CoSi_2$ layers. The self-assembled alkyl monolayer was deposited on the BML substrate, and its IRRAS was measured in the wide frequency range from stretching to bending regions.

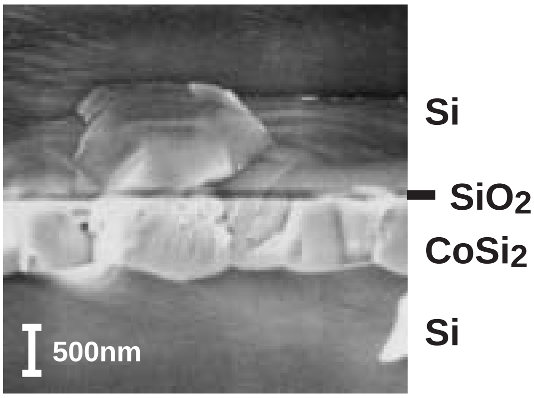

Figure 1. Cross-sectional SEM image of fabricated BML substrate by using preliminary formation of thin SiO_2 layer on the SOI surface.

VI-E Integration of Bio-Functional Materials on Silicon

Integration of bio-functional materials such as lipids and proteins are expected to find important applications in biosensors, development of new medicines, and diagnosis of intractable diseases *etc*. In this project, we are investigating the area selective modification of Si surfaces by depositing the self-assembled alkyl monolayers, and the integration of lipid bilayers supporting channel proteins keeping their bio-activities. Our special interests are developing “protein transistors” and co-integrating them together with the Si MOS FETs on the same Si chip.

VI-E-1 Deposition of Lipid DPPC Monolayer on SiO_2 Surface Using OTS Self-Assembled Monolayer Islands as Anchor Molecules

TAKIZAWA, Morio; KIM, Yong Hoon; TERO, Ryugo; URISU, Tsuneo

Bilayer lipid membranes (BLMs) supported on the solid surface are attractive research target from the viewpoint of application to the biosensors. The stability of the membrane can be increased significantly by using the *anchor molecules*. We have investigated the deposition of dipalmitoylphoshatidylcholine (DPPC) monolayer on SiO_2 surface using *n*-octadecyltrichlorosilane (OTS) self-assembled monolayer (SAM) islands as anchor molecules. After deposition of OTS SAM islands on SiO_2 surface, the DPPC monolayer was transferred to the surfaces by Langmuir-Blodgett method. The surface morphology observed by AFM shows that the flat DPPC monolayer is area-selectively deposited almost completely on the hydrophilic SiO_2 surface. On the hydrophobic OTS SAM surface, DPPC molecules were not observed as a form of monolayer. Bright protrusions were observed on and at the edges of the OTS islands, suggesting excess DPPC molecules accumulate and form three-dimensional islands. These results indicate that the OTS SAM islands have a potential of effective anchor molecules in DPPC BLM depositions on SiO_2 surfaces.

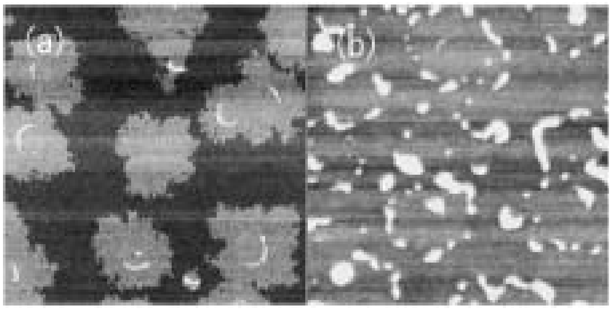

Figure 1. 5 μm × 5 μm AFM images of (a) OTS SAM islands and (b) DPPC monolayer deposition on OTS SAM/SiO_2 surface.

VI-E-2 Self-Assembled Monolayers on H-Si (111) Surfaces Studied by AFM Deposition of Undecenoic Acid

LI, Yanjun; TERO, Ryugo; NAGASAWA, Takayuki; NAGATA, Toshi; URISU, Tsuneo

A large number of studies have been conducted on the self-assembled monolayers (SAMs) from the view points of structure, formation process, and physical properties, for it is one of the promising candidates in applications such as adhesion promotion, surface modifications, surface protective films and the fabrication of devices such as field effect transistors.[1)–3)] The alkyl SAMs on Si substrates are relatively new topis and, among them, deposition of SAMs with a reactive group such as –COOH is especially interesting,[3)] since easiness of successive chemical treatments has potential applications to area selective immobilization of many kinds of bio-functional materials which is a key technology in the bioelectronics device fabrications. In the present work, the undecenoic acid (CH_2=CH-C_8H_{16}-COOH) SAMs were deposited on the hydrogen-terminated Si (111) surface, and the surface morphology was successfully observed for the first time by AFM.

The B-doped *p*-type Si(111) wafers with a resistivity in the rang of 8.4–8.9 Ω cm were cleaned, thermally oxidized and after removal of the oxide layer, the undecenoic acid SAM layer was deposited and AFM observation was performed. The wafer cleaning process was wet method as follows; (1) H_2O_2:H_2SO_4 = 1:4 → NH_4OH:H_2O_2:H_2O = 1:4:20 → diluted HF treatments, (2) HCl:H_2O_2:H_2O = 1:1:6 → diluted HF treatments. In each step, copious rinsing with ultrapure water, (3) oxidation of the Si sample at 1000 °C for one hour, (4) removal of the thermal oxide layer by HF (2%) solution, and (5) the etching of the Si sample by the solution of NH_4F:NH_4OH (*pH* = 8) for 5 min. Then the H-terminated Si sample was immediately placed in the distilled the undecenoic acid solution. The deposition process was as follows: (1) bubbling of the undecenoic acid solution by N_2 gas for 30 min at RT. (2) dipping of the Si sample into the solution with continuous N_2 bubbling for 30 min at RT. (3) heating of the solution at 200 °C for requesting time with continuous N_2 bubbling, (4) cooling down to RT, and (5) rinsing of the sample by methanol and propanol. After these processes, the sample surface morphology was investigated by AFM in the tapping mode.

Figure 1(a) shows the AFM image of the Si sample surface just after the cleaning process. The step edges are clearly observed. Figures 1(b) and (c) show the AFM images after the undecenoic acid deposition for 20 min. The island growth was confirmed on the Si(111) terraces, and the islands show unique hexagonal shapes, which is considered to be the reflection of the deposition mechanisms. We will make a detailed analysis about the AFM data in the succeeding research.

References

1) J. B. Brzoska, N. Shadhidzadch and F. Rondclcz, *Nature* **360**, 719–721 (1992).
2) A. B. Sieval, A. L. Demirel, J. W. M. Nissink, M. R. Linford, J. H. ven der Maas, W. H. de Jeu, H. Zuilhof and E. J. R. Sudholter, *Langmuir* **14**, 1759–1768 (1998).
3) S. D. More, H. Graaf, M. Baune, C. Wang and T. Urisu, *Jpn. J. Appl. Phys.* **41**, 4390–4394 (2002).

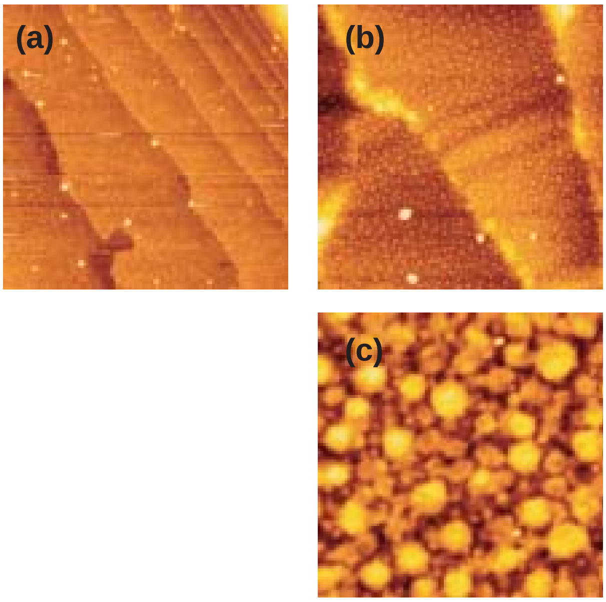

Figure 1. AFM images of the Si(111) sample surface, (a) just after the cleaning (800 μm × 800 μm) (b) after the undecenoic acid deposition (4 μm × 4 μm) and (c) in high magnification of (b) (800 nm × 800 nm).

VI-E-3 Characterization of Dipalmitoylphosphatidylcholine (DPPC)/Cholesterol Langmuir-Blodgett Monolayers by AFM and FT-IR

KIM, Yong Hoon; TAKIZAWA, Morio; URISU, Tsuneo

In advent of bio-nano technology, many experimental approaches have been performed to fabricate biosensors mimicking the ion channel system of cell membranes. In such system, intensity and lifetime of the ion channel current largely depend on membrane properties. Cholesterol is one of the major constituents in membranes and diminishes the gel to liquid crystalline phase transition. the chemical and physical properties and formation of the liquid-ordered phase (L_O), occurring at a certain cholesterol concentration, have been of considerable interest because the studies of this phase can provide important information related to the numerous biological functions in cell membranes, including signal transductions to immune systems and the activity of membrane proteins

It is the aim of this study to examine interactions of cholesterols with L_α phase of DPPC monolayer prepared by the Langmuir-Blodgett method. We have focused on effects of cholesterols, causing the formation of L_O phase, in relation to the conformational order of acyl chains of mixed (DPPC/cholesterol) monlayers and the behavior of phase separations in combination with FT-IR and AFM, respectively.

VI-F Photoionization and Photodissociation Dynamics Studied by Electron and Fluorescence Spectroscopy

Molecular photoionization is a major phenomenon in vacuum UV excitation and provides a large amount of information on fundamental electron-core interactions in molecules. Especially, neutral resonance states become of main interest, since they often dominate photoabsorption cross sections and lead to various vibronic states which are inaccessible in direct ionization. We have developed a versatile machine for photoelectron spectroscopy in order to elucidate dynamical aspects of superexcited states such as autoionization, resonance Auger decay, predissociation, vibronic couplings, and internal conversion. Two-dimensional photoelectron spectroscopy, allows us to investigate superexcited states in the valence excitation region of acetylene, nitric oxide, carbonyl sulfide, sulfur dioxide and so on. In a two-dimensional photoelectron spectrum (2D-PES), the photoelectron yield is measured as a function of both photon energy $E_{h\nu}$ and electron kinetic energy E_k (binding energy). The spectrum, usually represented as a contour plot, contains rich information on photoionization dynamics.

Photofragmentation into ionic and/or neutral species is also one of the most important phenomena in the vacuum UV excitation. In some cases, the fragments possess sufficient internal energy to de-excite radiatively by emitting UV or visible fluorescence. It is widely accepted that fluorescence spectroscopy is an important tool to determine the fragments and to clarify the mechanisms governing the dissociation processes of diatomic and polyatomic molecules. For several years we have concentrated upon fluorescence spectroscopy of H_2O in the photon energy region of 15–55 eV.

VI-F-1 Dissociation Mechanism of H_2O into $OH^+(\tilde{A}^3\Pi_\Omega)$ + H(n = 1) Manifested by Ultraviolet Dispersed Spectroscopy

MITSUKE, Koichiro

The photofragmentation of H_2O has been studied by fluorescence spectroscopy at photon energies between $h\nu$ = 16.9–54.5 eV. The primary photon beam was monochromatized undulator radiation supplied from BL3A2 of the UVSOR facility. The fluorescence in the wavelength range of 280–720 nm was dispersed with an imaging spectrograph.[1)] Figure 1 shows the fluorescence excitation spectrum for the (0,0) vibrational band of the $OH^+(\tilde{A}^3\Pi_\Omega \rightarrow \tilde{X}_3\Sigma^-)$ transition. The intensity shows a slow onset at 25.5 ± 0.3 eV. This value is much higher than the dissociation limit of 21.5 eV and can be interpreted in terms of a highly repulsive potential energy surface of the excited H_2O^+ state along the dissociation coordinate. The correlation diagram of H_2O^+ proposed by Appell and Durup[2)] predicts that the $OH^+(\tilde{A}^3\Pi_\Omega)$ + H(n = 1) limit correlates with a 2-hole 1-particle $^2A_1$ state of H_2O^+ with the electronic configuration of $[(1b_1)^{-2}(4a_1)^1]$. This doubly excited $H_2O^+(^2A_1)$ state was reported to be located at 27.6 ± 1 eV with respect to $H_2O(\tilde{X}^1A_1)$ in the Franck-Condon region. This vertical ionization energy rationalizes the present observation that the $OH^+(\tilde{A}^3\Pi_\Omega \rightarrow \tilde{X}^3\Sigma^-)$ band system begins to appear at $h\nu$ = 25.5 eV.

References

1) K. Mitsuke, *J. Chem. Phys.* **117**, 8334–8340 (2002).
2) J. Appell and J. Durup, *Int. J. Mass Spectrom. Ion Phys.* **10**, 247–265 (1972/73).

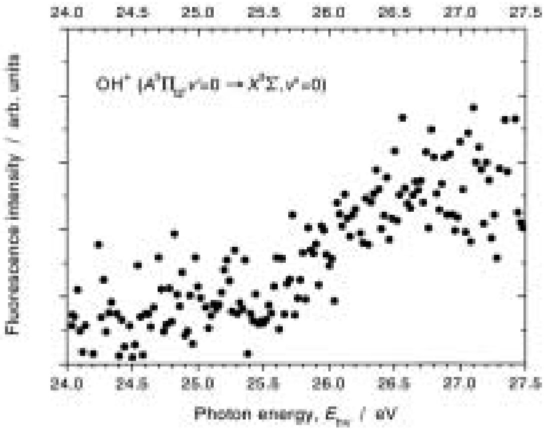

Figure 1. Fluorescence excitation spectrum for the (0,0) vibrational band of the $OH^+(\tilde{A}^3\Pi_\Omega \rightarrow \tilde{X}^3\Sigma^-)$ transition. The resolution of the synchrotron radiation was 2.4 Å.

VI-F-2 Autoionization of the Rydberg States Converging to $HI^+(\tilde{A}^2\Sigma^+_{1/2})$ below $h\nu$ = 12.7 eV

HIKOSAKA, Yasumasa[1]; MITSUKE, Koichiro
([1]Inst. Mater. Struct. Sci.)

[*J. Chem. Phys.* submitted]

Two-dimensional photoelectron spectroscopy of hydrogen iodide has been performed in the $E_{h\nu}$ range of 11.10–14.85 eV, in order to clarify autoionization mechanisms of the Rydberg states HI*(R_A) converging to $HI^+(\tilde{A}^2\Sigma^+_{1/2})$. The 2D-PES exhibits extensive vibrational excitation of $HI^+(\tilde{X}^2\Pi_{3/2}, v^+)$ over a $E_{h\nu}$ region from ~ 12 to 13.6 eV. The v^+ excitation below 12.7 eV is attributable to autoionizing features of the $5d\pi$ HI*(R_A) state. The potential energy curves of HI* and HI^+ are illustrated in Figure 1, where the curves of HI^+ are adopted from the literature.[1)] Superexcitation and subsequent autoionization is usually governed by the Franck-Condon principle. Since the wave functions for excited vibrational levels have large amplitudes near the potential wall, superexcitation into 5$d\pi$ HI*(R_A) affords population to a few vibrational levels whose classical turning points at the repulsive branch of 5$d\pi$ HI*(R_A) are included within the Franck-Condon region for transitions from HI($\tilde{X}^1\Sigma^+$). Then autoionization of these levels occurs either at near the repulsive branch or at the attractive branch, unless the lifetime with respect to autoionization is much shorter than the vibrational period of the 5$d\pi$ state. The extensive vibrational excitation at $E_{h\nu}$ < 12.7 eV can be accounted for by autoionization at the attractive branch.

Reference

1) A. J. Cormack, *et al.*, *Chem. Phys.* **221**, 175–188 (1997).

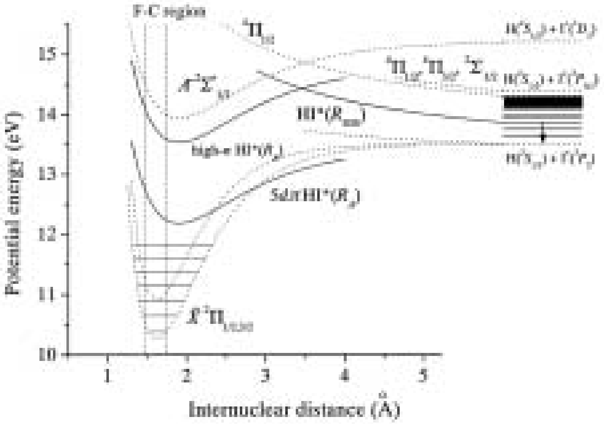

Figure 1. Schematic diagram for the potential energy curves of HI and HI$^+$. The solid and dashed lines designate the Rydberg and ionic states, respectively. The potential energy curves of HI*(R_A) states are assumed to have the same shape as those of HI$^+$($\tilde{A}^2\Sigma^+{}_{1/2}$). The term values used for the 5$d\pi$ and high-n Rydberg states are 1.76 and 0.44 eV, respectively. The Franck-Condon region is located between the two dashed vertical lines.

VI-F-3 Autoionization and Predissociation of the Rydberg States Converging to HI$^+$($\tilde{A}^2\Sigma^+{}_{1/2}$) at $h\nu$ = 13.2–13.6 eV

HIKOSAKA, Yasumasa[1]**; MITSUKE, Koichiro**
([1]Inst. Mater. Struct. Sci.)

The 2D-PES of HI at $E_{h\nu}$ = 13.2–13.6 eV has been closely studied to understand dynamical properties on autoionization and predissociation of HI*(R_A) (see also Theme VI-F-2). The v^+ distribution of HI$^+$($\tilde{X}^2\Pi_{3/2}$) shows an interesting left-side up pattern up to v^+ ~ 12. Namely, the relative population for a given v^+ reaches a maximum at $E_{h\nu} = E_{h\nu}^{\max}$ whose value increases with increasing v^+. At first sight one would presume that this vibrational pattern results from autoionization of high-n HI*(R_A) Rydberg states with n » 5.

Figure 1 shows the constant-ionic-state (CIS) spectra for v^+ = 0–3 of HI$^+$($\tilde{X}^2\Pi_{3/2}$) extracted from the 2D-PES. Panel (a) shows a broad resonance peak due to autoionization of 5$d\pi$ HI*(R_A). With increasing v^+ the spectral features spread from ~ 12.0 to ~ 13.3 eV and become complicated as seen from the other three Panels. At v^+ ≥ 3 the whole resonance splits into two broad peaks. The peak lying at higher energy shifts its maximum position from ~ 13.1 eV at v^+ = 3 to ~ 13.5 eV at v^+ = 12, being consistent with the left-side up pattern. At $E_{h\nu}$ = 13.2–13.6 eV, the integrated intensity for v^+ = 1 calculated from Figure 1(a) is no more than 4% of that for v^+ = 0. This ratio is much smaller than that at $E_{h\nu}$ = 12.2–12.7 eV, which implies that simple autoionization of the high-n HI*(R_A) states occur less efficiently than their conversion into predissociating repulsive states HI*(R_{Dis}). Then there is a probability that the system is converted from HI*(R_{Dis}) to low-n HI*(R_A) through avoided curve crossings. Autoionization of low-n HI*(R_A) states, such as the 5$d\pi$ state; produced by double conversion can provide populations of HI$^+$($\tilde{X}^2\Pi_{3/2,1/2}$) at higher v^+ than expected from the Franck-Condon factors between HI($\tilde{X}^1\Sigma^+$) and HI*(R_A). From the relation between the potential energy curves of low-n HI*(R_A) and HI$^+$($\tilde{X}^2\Pi_{3/2}$), autoionization can proceed mostly from the repulsive branch (see Figure 1 in Theme VI-F-2). The higher the n value of the primary high-n HI*(R_A) state becomes, the more the low-n HI*(R_A) state resulting from double conversion is vibrationally excited. Consequently, autoionizing transition occurs at a shorter nuclear distance and the final vibrational distribution of HI$^+$($\tilde{X}^2\Pi_{3/2,1/2}$) shifts to higher v^+. The left-side up pattern at $E_{h\nu}$ = 13–13.7 eV in the 2D-PES obviously supports this expectation.

Reference

1) Y. Hikosaka and K. Mitsuke, *J. Chem. Phys.* submitted.

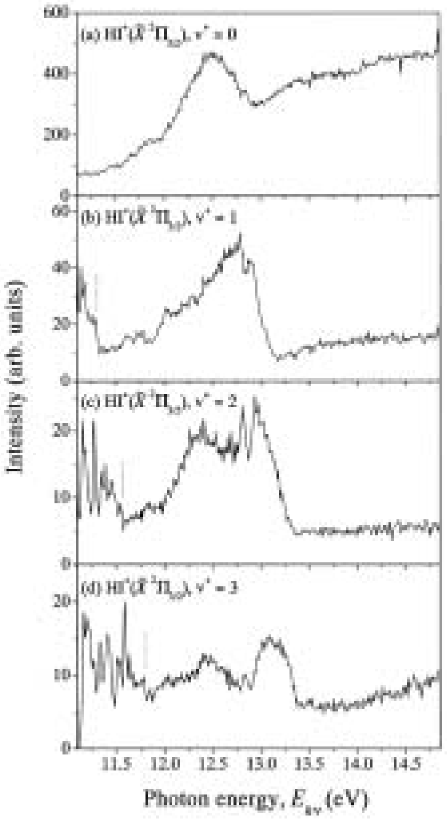

Figure 1. CIS spectra for the formation of v^+ = 0–3 vibrational levels of HI$^+$($\tilde{X}^2\Pi_{3/2}$), which are extracted from the 2D-PES. The ionization energies for the v^+ = 1, 2 and 3 levels of HI$^+$($\tilde{X}^2\Pi_{1/2}$) are indicated by the dotted lines in the spectra for v^+ = 1, 2 and 3, respectively.

VI-G Vacuum UV Spectroscopy Making Use of a Combination of Synchrotron Radiation and Laser

There is a growing interest in combining synchrotron radiation (SR) with the laser, since high resolution or ultrafast lasers are expected to open a new field for studies on dynamical behaviors of excited molecules in the VUV or soft X-ray region. Nevertheless, only a few attempts have been made on pump-probe experiments of gas-phase molecules using SR and a laser: photoelectron spectroscopy of atomic iodine produced from I_2 (Nahon *et al.*, 1990, 1991), photoelectron spectroscopy of N_2 and HCN produced from *s*-tetrazine (Nahon *et al.*, 1992), and photoionization of atomic iodine produced from CH_3I (Mizutani *et al.*, 1997). In UVSOR we have developed ultraviolet laser system which synchronizes precisely with the SR pulses from the storage ring to take maximum advantage of the features of the laser, *i.e.* its excellent spectral and temporal resolution, we employed the laser in detecting and analyzing products resulting from VUV or soft X-ray photoexcitation. The following combination studies have been performed: (1) two-photon ionization of helium atoms studied as the prototype of the time-resolved experiment (Mizutani *et al.*, 1997), (2) laser induced fluorescence (LIF) excitation spectroscopy of $N_2^+(X\ ^2\Sigma_g^+)$ ions or $CN(X\ ^2\Sigma^+)$ radicals produced by SR photoionization of N_2, N_2O, or CH_3CN (Mizutani *et al.*, 1998; Mitsuke *et al.*, 1998, 2001). This year another combination work commences as a new project, that is, SR photodissociation of vibrationally excited molecules prepared with irradiation of visible or infrared single frequency laser.

VI-G-1 Development of the Laser–SR Combination System for Photodissociation Studies of Highly Vibrationally Excited Molecules

MITSUKE, Koichiro

It is possible that the initial vibrational excitation in a molecule influences the chemical branching, if two different photodissociation channels are accessible. Much attention has been focused on the pioneering work of Crim and his collaborators,$^{1)}$ who could accomplish the selective bond-breaking of heavy water, HOD. Very recently, Akagi and coworkers$^{2)}$ reported that deuterized ammonia NHD_2 in the fourth N–H stretching overtone preferentially photodissociates into the ND_2 + H channel. In these two studies UV lasers were employed for vibrationally mediated photodissociation.

Instead, we are planning to use synchrotron radiation (SR) to promote vibrationally excited molecules to electronically excited states in the vacuum UV region. The main objectives are as follows: (1) Elucidating the properties of dissociative states by sampling a wide range of their potential energy surfaces, such as dynamics determining the final-state distributions of the products, nonadiabatic transitions on dissociation, and assignments and characterization of unknown multiply-excited states produced by Auger decay from core-excited states. (2) Aiming at more universal “vibrational state-specific” rupture of chemical bonds, which could be realized by changing the overlap between the wave-fucntions of the upper-state continuum and that of the ground state.

References

1) R. L. Vander Wal, J. L. Scott and F. F. Crim, *J. Chem. Phys.* **92**, 803–805 (1990).
2) H. Akagi, K. Yokoyama and A. Yokoyama, *J. Chem. Phys.* **118**, 3600–3611 (2003).

VI-G-2 Photodissociation of Vibrationally Excited H_2O in the $4\nu_{O-H}$ Region into $OH^+(X^3\Sigma^-)$ + H(*n* = 1)

MITSUKE, Koichiro; KOU, Junkei; MORI, Takanori

We have searched appropriate excited states through which photodissociation of vibrationally excited molecules can be investigated, on the basis of the correlation diagram in Figure 1 that we proposed in the dispersed fluorescence study for the extreme UV photoionization of H_2O.$^{1)}$ First, we tackled the two $^2A_1$ states which correlate with the $OH^+(A^3\Pi_\Omega)$ + H(*n* = 1) and OH $(A^2\Sigma^+)$ + H^+ limits. Since the two states are highly repulsive, it is possible that significant decrease in the appearance energy is observed for the formation of $OH^+(A^3\Pi_\Omega)$ or $OH(A^2\Sigma^+)$ from vibrationally excited molecules. Here, spontaneous emission from these photofragments are detected.

A continuous titanium-sapphire laser was used in the wavenumber range between 13814–13819 cm^{-1}, with its bandwidth of 4×10^{-4} cm^{-1}. This energy range corresponds to excitation of the third O–H stretching overtone of water. However, when the visible laser was introduced together with SR, no additional peak feature of emission bands was detected in the dispersed spectra. Then we shifted the target to the dissociation channel of $OH^+(X^3\Sigma^-)$ + H(*n* = 1). The OH^+ ion was detected using mass spectrometry at SR photon energies near the dissociation threshold of 18.05 eV with respect to the neutral ground state. The difference between the normalized signal ion counts with and without the visible laser appears to exhibit multi-modal reflection structures due to the nodes of the vibrational wave function of the $4\nu_{O-H}$ stretch overtone of H_2O.

Reference

1) K. Mitsuke, *J. Chem. Phys.* **117**, 8334–8340 (2002).

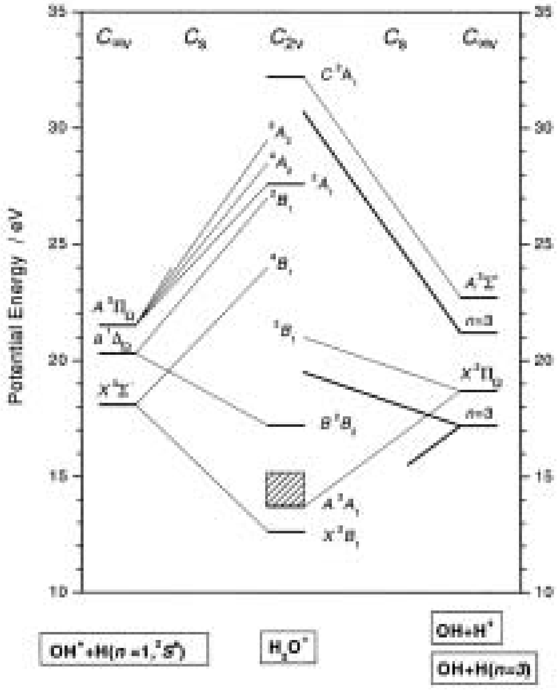

Figure 1. Correlation diagram between H_2O^+ and $OH^+ + H$ and between H_2O^+ and $OH + H^+$.

VI-H Extreme UV Photoionization Studies of Polyatomic Molecules and Fullerenes by Employing a Grazing-Incidence Monochromator

On the beam line BL2B2 in UVSOR a grazing incidence monochromator has been constructed which supplies photons in the energy region from 20 to 200 eV [M. Ono, H. Yoshida, H. Hattori and K. Mitsuke, *Nucl. Instrum. Methods Phys. Res., Sect. A* **467-468**, 577–580 (2001)]. This monochromator has bridged the energy gap between the beam lines BL3B and BL4B, thus providing for an accelerating demand for the high-resolution and high-flux photon beam from the research fields of photoexcitation of inner-valence electrons, *L*-shell electrons in the third-row atom, and 4*d* electrons of the lanthanides.

Since 2001 we have tried taking photoion yield curves of fullerenes. Geometrical structures and electronic properties of fullerenes have attracted widespread attention because of their novel structures, novel reactivity, and novel catalytic behaviors as typical nanometer-size materials. Moreover, it has been emphasized that the potential for the development of fullerenes to superconductors (T_c ~ 50 K) and strong ferromagnetic substances is extremely high. In spite of such important species spectroscopic information is very limited in the extreme UV region, which has been probably due to difficulties in obtaining enough amount of sample. The situation has been rapidly changed in these few years, since the techniques of syntheses, isolation, and purification have been advanced so rapidly that appreciable amount of fullerenes is obtainable from several distributors in Japan.

VI-H-1 Anisotropy of Fragment Ions from SF_6 by Photoexcitation between 23 and 210 eV

ONO, Masaki[1]; MITSUKE, Koichiro
([1]Louisiana State Univ.)

[*Chem. Phys. Lett.* **366**, 595–600 (2002)]

The anisotropy of the ionic photofragments produced from SF_6 has been measured using synchrotron radiation in the range of 23–210 eV. Despite the highly symmetrical molecule a strong anisotropy is observed below ~ 35 eV. The behavior of the asymmetry parameter involving all the fragment ions has been interpreted by simulation using partial oscillator strengths for the formation of individual species. Only SF_5^+ ions produced via superexcited states of valence type are assumed to have an anisotropic angular distribution. The observed decrease in the asymmetry parameter with increasing photon energy can be ascribed to the dominance of direct photoionization and the decrease in the branching ratio for SF_5^+ formation.

VI-H-2 Kinetic Energy Distribution and Anisotropy of Fragment Ions from SF_6 by Photoexcitation of a Sulfur 2*p*-Electron

ONO, Masaki[1]; MITSUKE, Koichiro
([1]Louisiana State Univ.)

[*Chem. Phys. Lett.* in press]

The kinetic energy (KE) distribution and asymmetry parameter β have been studied for photofragmentation of SF_6 near the sulfur 2*p* ionization edges at 170–208 eV by using synchrotron radiation. The relative yield of fast ions with KE > 5 eV is larger in the post-edge than in the pre-edge region (see Figure 1), whereas β of such ions is lower in the post-edge region. The β curve shows a sudden drop from 0.06–0.07 to zero near the edges and remains constant thereafter. These results are ascribed to *LVV* Auger decay occurring above the edges leading to SF_6^{2+} and SF_6^{3+} transiently. At KE > 2 eV the distribution curve for the S $2p \rightarrow 6a_{1g}$ resonance transition behaves in the same manner as that for the valence-electron ionization at 170 eV. This agreement, together with a similarity in β, suggests that the S $2p \rightarrow 6a_{1g}$ resonance and valence-electron ionization suffer similar formation pathways leading to ions with high KE.

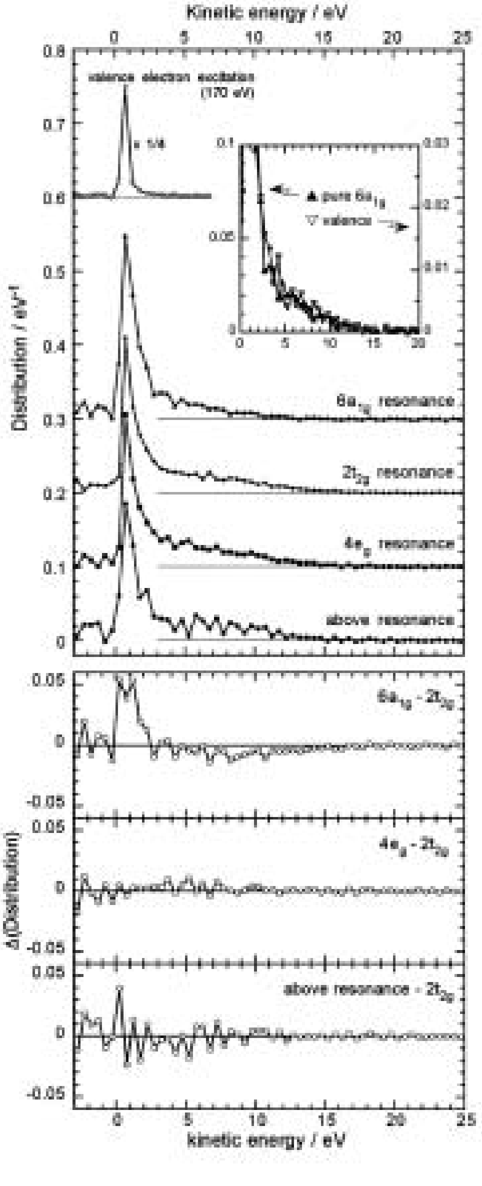

Figure 1. Upper panel: Kinetic energy distributions for sheer S 2*p*-electron excitation after subtracting the contributions of valence-electron photoionization. Inset shows expansion of the two distributions for the $6a_{1g}$ resonance at $h\nu = 173.5$ eV and valence-electron ionization at 170 eV. Lower panel: Differences in distribution between the $2t_{2g}$ resonance and one of the three excitation energies (the $6a_{1g}$, $4e_g$ resonance and above the resonance).

VI-H-3 Molecular- and Atomic-Like Photoionization of C_{60} in the Extreme Ultraviolet

KOU, Junkei; MORI, Takanori; ONO, Masaki[1]; HARUYAMA, Yusuke[2]; KUBOZONO, Yoshihiro[3]; MITSUKE, Koichiro
([1]Louisiana State Univ.; [2]Okayama Univ.; [3]IMS and Okayama Univ.)

[*Chem. Phys. Lett.* **374**, 1–6 (2003)]

Photoion yield spectra of C_{60} in the gas phase have been measured from 23 to 180 eV by using synchrotron radiation. Two peaks at 26 and 34 eV and a flat area ranging from 40 to 50 eV are newly observed in the higher energy side of the giant resonance at ~ 20 eV, as shown in Figure 1. These features are assigned as resulting from the shape resonance on photoionization of valence electrons of C_{60} with large orbital angular momenta: the ionized electron is temporarily trapped inside a centrifugal barrier. Above ~ 50 eV the yield curve shows a steady decrease with increasing photon energy like the photoabsorption cross section of atomic carbon. Thus, the spectrum is considered to be determined by photoionization of the 2*s* orbitals of the carbon atoms.

Reference

1) P. Colavita, *et al.*, *Phys. Chem. Chem. Phys.* **3**, 4481–4487 (2001).

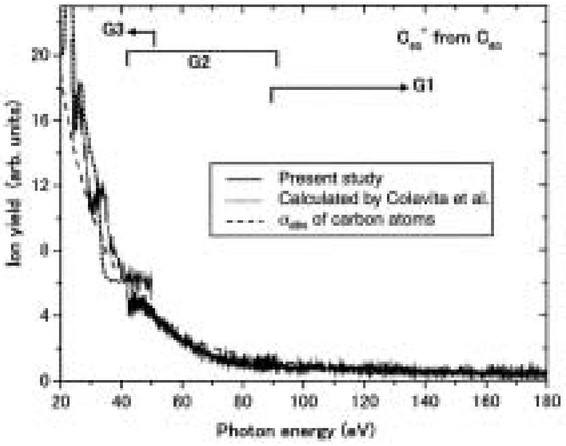

Figure 1. Solid curves: photoion yield of C_{60}^+ from C_{60} (present study). The dotted and dashed curves indicate the calculated photoabsorption cross sections of C_{60} and sixty carbon atoms, respectively, taken from Reference 1).

VI-H-4 Development of a Photoionization Spectrometer for Accurate Ion Yield Measurements from Gaseous Fullerenes

MORI, Takanori; KOU, Junkei; ONO, Masaki[1]; HARUYAMA, Yusuke[2]; KUBOZONO, Yoshihiro[3]; MITSUKE, Koichiro
([1]Louisiana State Univ.; [2]Okayama Univ.; [3]IMS and Okayama Univ.)

[*Rev. Sci. Instrum.* **74**, 3769–3773 (2003)]

A photoionization spectrometer has been developed for measuring the ion yields for fullerenes in the photon energy range of 23–200 eV (see Figure 1). Gaseous fullerenes were supplied from a high-temperature oven, ionized by irradiation of monochromatized synchrotron radiation and detected after analysis with a time-of-flight mass spectrometer. The fluxes of the synchrotron radiation and fullerene beams were monitored concurrently with the acquisition of the ion signal counts in order to obtain reliable photoionization efficiency curves. The performance of the apparatus was examined by measuring the efficiency curve of C_{60}^{+} produced from C_{60}. The spectrum demonstrated better statistics than the previous results in the same photon energy region. Three distinct features were newly observed in the higher energy side of the prominent resonance at ~ 20 eV.

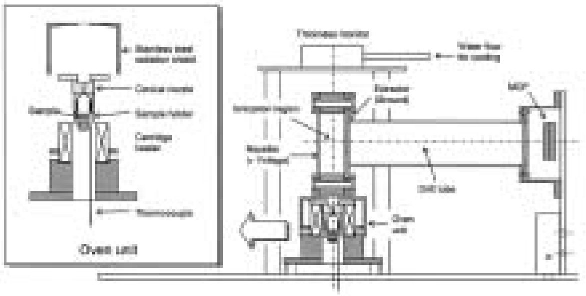

Figure 1. Apparatus of the photoionization spectrometer and an expansion of the oven unit.

VI-H-5 Production of Doubly Charged Ions in Valence Photoionization of C_{60} and C_{70} at $h\nu$ = 25–150 eV

KOU, Junkei; MORI, Takanori; S. V. K. Kumar[1]; HARUYAMA, Yusuke[2]; KUBOZONO, Yoshihiro[3]; MITSUKE, Koichiro
([1]IMS and Tata Inst. Fund. Res.; [2]Okayama Univ.; [3]IMS and Okayama Univ.)

[*J. Chem. Phys.* submitted]

Relative partial photoionization cross sections for production of singly and doubly charged ions of C_{60} and C_{70} have been measured at $h\nu$ = 25–150 eV. Figure 1 shows the photoionization yield curves of C_{60} for the formation of C_{60}^{n+} (n = 1 and 2). Since the yields for multiply charged ions with $n \geq 3$ are not significant in this energy region, one can regard the composite spectrum obtained by summing up the yields for C_{60}^{+} and C_{60}^{2+} as the total photoionization yield of C_{60} or, to a good approximation, the total photoabsorption cross section of C_{60}. There are three peaks at $h\nu$ = 26, 34, and 49 eV in the composite spectrum. The total photoabsorption spectrum theoretically determined by Colavita and cowokers1) is depicted by the dotted curve in Figure 1. A comparison of the present total photoionization yield with the reported photoabsorption spectrum shows a large disagreement, probably because of the contribution of C_{60}^{2+} produced through the mechanism that has not been taken into account1) in the *ab initio* calculations. The most probable pathway to produce C_{60}^{2+} is considered to be spectator Auger decay of shape resonance states followed by cascade or electron tunneling, because there are many shape resonance states at various photon energies. In contrast, resonace Auger processes have been disregarded in the calculations.1) The partial and total photoionzation yield curves of C_{70} are similar to those of C_{60}. Ratio of the yields of C_{60}^{2+}/C_{60}^{+} and C_{70}^{2+}/C_{70}^{+} are found to be larger than unity at $h\nu > 50$ eV. The observed yield curves and ratios quite differ from those reported in the electron impact ionization of C_{60} and C_{70}.

Reference

1) P. Colavita, *et al.*, *Phys. Chem. Chem. Phys.* **3**, 4481–4487 (2001).

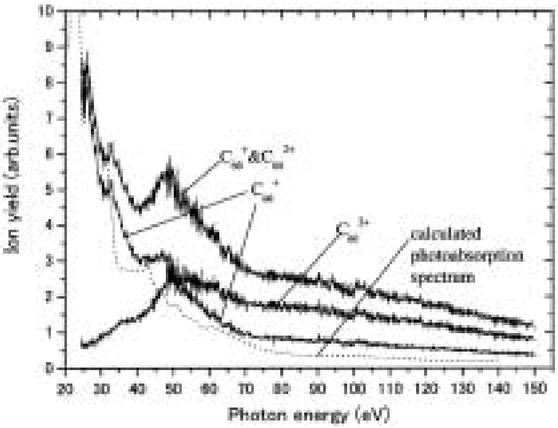

Figure 1. Partial and total photoionization yield curves of C_{60}.